Received July 27, 2020, accepted August 12, 2020, date of publication August 18, 2020, date of current version August 27, 2020.

Digital Object Identifier 10.1109/ACCESS.2020.3017482

A Novel Power Spectrum-Based Sequential Tracker for Time-Variant Radio Propagation Channel

TIANQI WU[1], (Graduate Student Member, IEEE), XUEFENG YIN[1], (Member, IEEE), AND JUYUL LEE[2], (Senior Member, IEEE)

[1]College of Electronics and Information Engineering, Tongji University, Shanghai 201804, China
[2]Electronics and Telecommunications Research Institute (ETRI), Daejeon 34129, South Korea

Corresponding author: Xuefeng Yin (yinxuefeng@tongji.edu.cn)

This work was supported in part by the National Natural Science Foundation of China (NSFC) General Project under Grant 61971313, and in part by the Institute for Information and Communications Technology Planning and Evaluation (IITP) Grant, Korean Government, under Grant 2017-0-00066.

ABSTRACT Cluster tracking is a mainstream approach for the study of time-variant channel characteristics. In the paper, we propose a power spectrum based sequential tracker (PSBST) to compensate for the disadvantages of existing cluster tracking algorithms. The proposed tracker identifies clusters via simple three-stage power spectrum processing. Furthermore, fuzzy c-means (FCM) algorithm is incorporated to separate clusters considering the overlapped clusters which may appear in the power spectrum. In terms of tracking, we implement Kalman filter to sequentially predict candidate ranges of tracked clusters in consecutive snapshots and simultaneously a novel gradient-based histogram of power (GBHOP) method is devised to determine the evolution of clusters. We also investigate the performance of the tracker by synthetic channel simulation. It demonstrates high accuracy and less computational time compared with the results derived from the existing cluster tracking algorithms. Besides, we verify applicability of the tracker by analyzing the field measurement conducted in vehicle-to-everything (V2X) scenario, and preliminary statistical characteristics for intra-cluster and inter-cluster parameters can be readily obtained in the sequel.

INDEX TERMS Time-variant radio channel, cluster tracking, power spectrum, fuzzy clustering, cluster detection, V2X.

NOMENCLATURE

$h(t,\tau)$	Time-variant channel impulse response
$P(m,n)$	Discrete scattering function
L	Number of candidate pixels
$\mathcal{S}$	Location set of candidate pixels
$\mathcal{S}_l$	Location of the lth candidate pixel
$\mathcal{S}_c$	Location of the cutoff pixel
$\mathcal{E}$	Neighbor set of the cutoff pixel
L'	Number of selected pixels after image denoising
$\mathcal{S}'$	Location set of selected pixels
P	Number of coarse segments
$\mathcal{S}'_p$	Location set of the pth coarse segment
$\mathcal{S}'_{p,i}$	Location of the ith pixel in the pth coarse segment
$\mathcal{S}''_{p,j}$	Location of the jth cluster center in the pth coarse segment
I_p	Number of pixels in the pth coarse segment
J_p	Number of clusters in the pth coarse segment
u_{ij}	Fuzzy membership of the ith pixel to the jth cluster
$\widetilde{u}_{ij}$	Normalized fuzzy membership
r	Membership coefficient
$\widetilde{\tau}_{t'}$	Observed fuzzy power weighted mean delay
$\widetilde{\nu}_{t'}$	Observed fuzzy power weighted mean Doppler
$\widetilde{\boldsymbol{\mu}}_{t'}$	Observed mean cluster state set
$\widetilde{\sigma}_{\tau,t'}$	Observed fuzzy power weighted delay spread
$\widetilde{\sigma}_{\nu,t'}$	Observed fuzzy power weighted Doppler spread
$\widetilde{m}$	Subpixel level column index of cluster center
$\widetilde{n}$	Subpixel level row index of cluster center
τ'	System resolution of delay
ν'	System resolution of Doppler
$\tau_{t'}$	Actual cluster delay
$\nu_{t'}$	Actual cluster Doppler
$\Delta\tau_{t'}$	Rate of change for cluster delay
$\Delta\nu_{t'}$	Rate of change for cluster Doppler
$\Theta_{t'}$	Cluster intrinsic parameter set

The associate editor coordinating the review of this manuscript and approving it for publication was Vittorio Degli-Esposti

$\mathbf{w}_{t'}$	Process noise vector
$\mathbf{v}_{t'}$	Measurement noise vector
$\mathbf{Q}$	Covariance matrix of $\mathbf{w}_{t'}$
$\mathbf{R}$	Covariance matrix of $\mathbf{v}_{t'}$
$\mathbf{A}$	State transition matrix
$\mathbf{H}$	Measurement matrix
$\mathbf{P}$	Estimation error covariance
$\mathbf{K}$	Kalman gain
T_d	Threshold of pixel-level distance
Y	Maximum number of pixels in one cluster
g	Number of bins in the histogram
d	Bin size of the histogram
$G(m, n)$	Gradient of the pixel
$\boldsymbol{h}_1$	Histogram of the previous cluster
$\boldsymbol{h}_2$	Histogram of the candidate cluster
$\mathrm{sim}(\cdot)$	Cosine similarity
T_s	Threshold of cosine similarity
$P_{\max}$	Maximum pixel power in the power spectrum
P_{tot}	Total sum of pixel powers in the power spectrum
K_{LOS}	LOS power factor

I. INTRODUCTION

Radio propagation channel is the essential of wireless communications system, and channel characteristics influence the performance of the whole system significantly. Hence it is necessary to give a deep insight into channel characteristics by means of measurement campaign or computer simulation in order to improve the performance of wireless communications system.

Stationary channel characteristics have been widely studied in various scenarios with different carrier frequencies. It is found that multipath components (MPCs) usually appear in distinct clusters which are defined as groups of MPCs with similar parameters such as delay, Doppler frequency, angle of arrival (AoA), angle of departure (AoD) and so on in the channel [1]–[3]. This concept has also been adopted by many channel models, for example, the classical Saleh-Valenzuela (S-V) model [4], the random-cluster channel model [5], the COST 2100 channel model [6], etc. The conventional methods to identify clusters are visual inspection [7] and automatic K-Means clustering algorithm with multipath component distance (MCD) [8]. However, cluster identification by these two methods becomes troublesome when MPCs from different clusters are close to each other. Furthermore, parameters of these MPCs are extracted from measurement data using high-resolution parameter estimation (HRPE) algorithm, e.g., space-alternating generalized expectation-maximization (SAGE) algorithm [9], and it occupies considerable computational complexity in practice.

Clustering provides an efficient way to comprehensively analyze the characteristics of radio propagation channel and construct the channel model. Nevertheless, the real-life channel is not usually tractable due to its nonstationarity especially in the intelligent transportation system (ITS) [10], [11]. Although parameters of radio propagation paths may markedly vary with time, there exists internal connection between MPCs in consecutive snapshots. In other words, the cluster in the nonstationary channel can be further regarded as a group of MPCs with similar properties, e.g., from the same transmitter [12] or the same scatterer [13]. Consequently, tracking attracts attention to analysis of the time-variant channel, and it can help reproduce the channel evolution between consecutive snapshots.

Early researches focus on tracking of individual radio propagation paths in multiple-input-multiple-output (MIMO) channel to observe the temporal variation of dominant paths. To this end, in [14] and [15], expectation-maximization (EM) and SAGE are respectively improved to track path parameters sequentially. Besides, extended Kalman filter (EKF) [16] and particle filter [17] are respectively combined with HRPE algorithms to track paths based on the predefined system model and received signals. However, MPCs generally appear in clusters, and it leads to the redundancy of tracking of individual MPCs. Lately, more researches pay attention to cluster tracking algorithms. To the best of our knowledge, these algorithms can be mainly categorized as three frameworks based on the order of clustering and tracking. First clustering last tracking (FCLT) and joint clustering-and-tracking are two common algorithm frameworks. The former identifies clusters in each snapshot using some clustering algorithm and then tracks clusters snapshot by snapshot based on their parameter characteristics, e.g., MCD [8] or total sum of distances [18]. Meanwhile, the latter framework first tracks the clusters or MPCs in the previous snapshot and then identifies clusters in the current snapshot based on the tracking results [19]–[21]. The other framework is first tracking last clustering (FTLC) which is presented in [22] and [23]. It identifies clusters considering the similarity of temporal evolution among scattering points or multipath trajectories. it is noteworthy that the methods mentioned above are generally time-consuming because of the parameter estimation or geometry information involved. Furthermore, the HRPE algorithm and clustering algorithm in these methods need indeterminate priori parameters such as the number of MPCs and number of clusters. These parameters are subjective and markedly influence the clustering.

In order to avoid these troublesome details, a new kind of algorithms represented by the power-angle-spectrum based clustering and tracking algorithm (PASCT) [24] recently emerges which identifies clusters via image processing of power spectrum and tracks clusters using image feature matching. In fact, this kind of algorithms is the application of computer vision in channel modeling. However, there are two main disadvantages in terms of the PASCT. For one thing, it also needs quite a few predefined variables which brings inconvenience to the algorithm implementation. For another, the clusters with relatively low power are easily neglected according to the framework of cluster recognition in the algorithm. Hence, we need to develop a new algorithm to compensate for the disadvantages of PASCT and

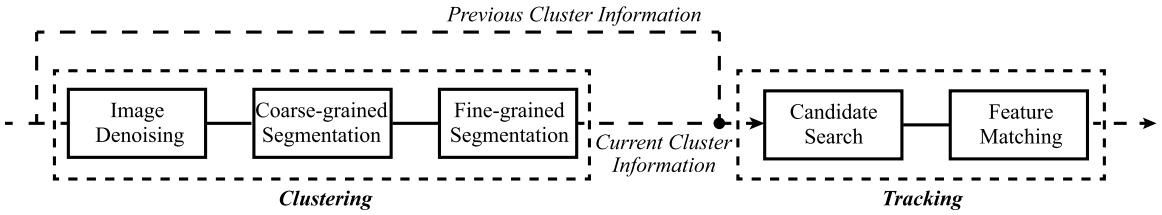

FIGURE 1. The flowchart of proposed PSBST.

give full play to the advantages of power spectrum based algorithm.

In this article, we propose a novel power spectrum based sequential tracker (PSBST) to promote the power spectrum based cluster tracking algorithm. The key contributions of our work are listed as below.

- PSBST can sequentially identify and track clusters in the time-variant channel. It needs less predefined parameters which increases stability of the tracker. In addition, it not only contributes to cluster characteristics analysis in the nonstationary channel, but also avoids the redundancy of tracking of individual MPCs proposed in [14]–[17].
- We implement a simple three-stage image processing in the framework of clustering. It can rapidly detect clusters compared with conventional HRPE based algorithms [18]–[23]. Moreover, it can completely identify clusters avoiding the cluster omission which happens in PASCT [24].
- To our knowledge, the overlap of clusters is not considered in existing cluster tracking algorithms. Hence, fuzzy c-means (FCM) algorithm is additionally incorporated into PSBST to separate clusters with fuzzy membership. Under the circumstances, clusters can be separated even when they are close to each other, which performs better than KPowerMeans based algorithms [8], [19]–[21].
- As for the framework of tracking, we use Kalman filter to predict candidate ranges of tracked clusters in a snapshot-by-snapshot way. Besides, a novel gradient-based histogram of power (GBHOP) method is devised to finally determine the evolution of clusters.
- We conduct the synthetic channel simulation to investigate performance of the tracker. The accuracy and computational time of PSBST are compared with those of PASCT [24] and the conventional KPowerMeans based cluster tracking algorithm (KPMCT) [8].
- We apply our tracker to the vehicle-to-everything (V2X) field measurement, and preliminary statistical characteristics for intra-cluster and inter-cluster parameters are obtained. The rationality of these results is verified compared with the results derived from KPMCT using the same data.

The organization of the paper is as follows. Section II introduces a comprehensive framework of the proposed PSBST. In Section III, performance of the tracker is investigated by means of simulation. Section IV presents experimental results of applying the tracker to the V2X field measurement. The conclusion is given in Section V.

II. PROPOSED SEQUENTIAL TRACKER

The proposed PSBST belongs to the category of FCLT and it is also divided into two steps, i.e., clustering and tracking as described in [8], [18] and [24]. The flowchart of PSBST is shown in Fig. 1. To sum up, given the current power spectrum, invalid areas with low power are firstly excluded in the image denoising step. Then individual power-concentrated areas are extracted and these areas are further separated into clusters respectively in the coarse-grained and fine-grained segmentation step. Finally, variation ranges of the tracked clusters are predicted based on previous cluster location information in the candidate search step and the evolution of clusters is determined combined with image features of previous clusters in the feature matching step. The proposed tracker is applicable to the MIMO channel as long as we obtain the spectrum. However, the design of MIMO sounder which can be effectively used in dynamic scenario is difficult to us for now, and we adopt SISO channel sounder for simplicity. Hence, in this section, we take the delay-Doppler power spectrum as example to elaborately introduce frameworks of clustering and tracking of the tracker.

A. FRAMEWORK OF CLUSTERING

Assuming that the channel in one snapshot with a short time satisfies wide-sense stationary uncorrelated scattering (WSSUS) [25], we apply Fast Fourier Transform (FFT) to the autocorrelation function of time-variant channel impulse response $h(t, \tau)$ with respect to time t. As a result, the discrete linear delay-Doppler power spectrum (also called as scattering function) at time instant t' can be obtained as

$$P(\tau_m, \nu_n; t') = \int \mathrm{E}[h^*(t', \tau_m)h(t'+\Delta t, \tau_m)]e^{-j2\pi\nu_n\Delta t}d\Delta t. \tag{1}$$

In this expression, $1 \le m \le M$ and $1 \le n \le N$ are respectively indices of discrete delay τ_m and Doppler frequency ν_n. For simplicity, these discrete parameters are generally with equal spacing and determined by the system resolution. Note that hereinafter the delay-Doppler spectrum $P(m, n)$ can be deemed as a gray image with $M \times N$ pixels where m and n are exactly indices of column and row, and therefore the location index of the pixel is denoted as (m, n).

The framework of clustering includes three stages, i.e., image denoising, coarse-grained segmentation and fine-grained segmentation. The illustrations of these stages are shown in Figs. 2 which are obtained from the tracker

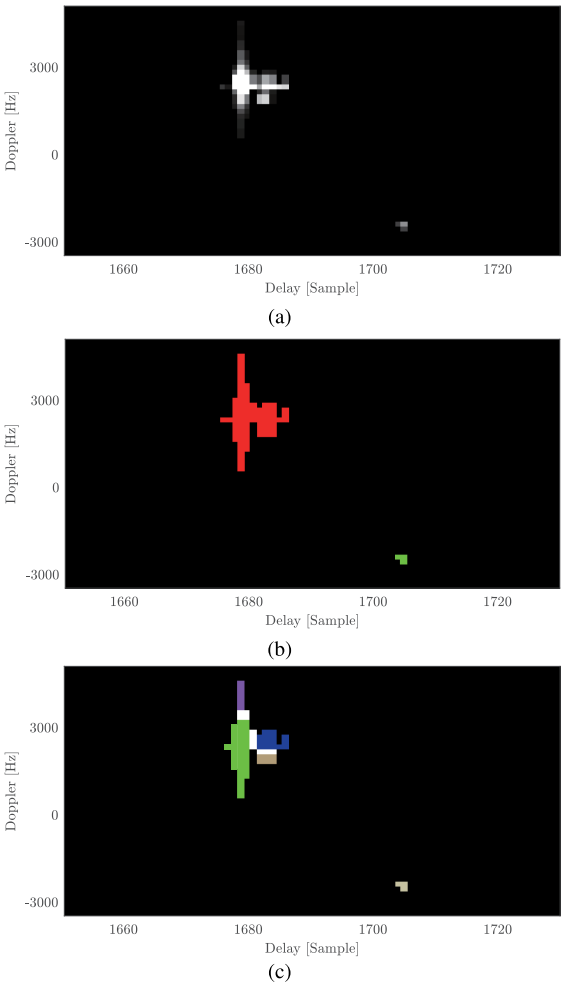

FIGURE 2. The illustrations of three stages in clustering: (a) Image Denoising. The brightness of pixels indicates the power and pixels in black are deemed noises. (b) Coarse-grained Segmentation. The coarse segments are represented by different colors. (c) Fine-grained Segmentation. Coarse segments are further divided into clusters in different colors. Moreover, the white pixels represent overlaps among these clusters.

application in Section IV. Note that we show images with a partial delay domain in order to have a clear view of segments.

1) IMAGE DENOISING

The initial power spectrum is composed of power-concentrated areas and noises that are out of power-concentrated areas. We need to exclude noises from the spectrum and retain power-concentrated areas in preparation for the next step. To this end, we firstly pick out the first L candidate pixels with the strongest powers considering that power of those areas is generally stronger than the noise level. Through our experiments, the empirical value of L can be one percent of the number of pixels in power spectrum, and it is sufficient to extract the whole pixels in power-concentrated areas. We also sort these candidate pixels with respect to the power in ascending order. The location index set of these sorted pixels is denoted as

$$\mathcal{S} = \{(m_l, n_l), l = 1, \ldots, L\} \tag{2}$$

where $\mathcal{S}_l = (m_l, n_l)$ indicates the location index of the lth pixel. Secondly, we check each pixel from the first to the Lth until finding the cutoff pixel with location index $\mathcal{S}_c = (m_c, n_c)$. Its neighbor set $\mathcal{E}$ satisfies

$$\begin{aligned} &\mathcal{E} \cap \mathcal{S} \neq \varnothing \\ &\mathcal{E} = \{(m_c \pm 1, n_c), (m_c, n_c \pm 1)\} \end{aligned} \tag{3}$$

where $\varnothing$ represents the empty set. Finally, we calculate the median of powers of the pixels whose location index is $\mathcal{S}_l, l \geq c$ so as to identify the dominant pixels in power-concentrated areas. Therefore, the pixels whose powers are stronger than the median are retained while the other pixels are considered as noises. In addition, in case of outliers, we need to remove the pixels whose neighbors' powers are all lower than the median from the remaining pixels. Fig. 2a displays the power spectrum after denoising where light areas indicate the finally selected L' pixels whose location index set is denoted as $\mathcal{S}'$.

2) COARSE-GRAINED SEGMENTATION

The pixels selected in the image denoising step constitute several individual power-concentrated areas. That is to say,

$$\begin{aligned} \mathcal{S}' &= \bigcup_{p=1}^{P} \mathcal{S}'_p \\ \mathcal{S}'_{p_1} \cap \mathcal{S}'_{p_2} &= \varnothing, \quad \forall p_1 \neq p_2,\ p_1, p_2 \in \{1, \ldots, P\} \end{aligned} \tag{4}$$

where P is the number of power-concentrated areas and $\mathcal{S}'_p$ represents the pth power-concentrated area. Furthermore, these areas are made up of adjoining pixels, i.e., the pixels in one area $\mathcal{S}'_p$ satisfy

$$\left\| \mathcal{S}'_{p,i} - \mathcal{S}'_{p,q} \right\|_{MT} \neq \infty,\ \forall \mathcal{S}'_{p,i}, \mathcal{S}'_{p,q} \in \mathcal{S}'_p \tag{5}$$

where $\|\cdot\|_{MT}$ is a Manhattan distance-type distance measure which is recursively defined as

$$\begin{aligned} &\left\| \mathcal{S}'_{p,i} - \mathcal{S}'_{p,q} \right\|_{MT} \\ &= \begin{cases} 0, & \text{if } \left\| \mathcal{S}'_{p,i} - \mathcal{S}'_{p,q} \right\|_{M} = 0 \\ 1, & \text{if } \left\| \mathcal{S}'_{p,i} - \mathcal{S}'_{p,q} \right\|_{M} = 1 \\ \min\limits_{\text{s.t. } \left\| \mathcal{S}'_{p,i} - \mathcal{S}'_{p,m} \right\|_{M} = 1} \left(1 + \left\| \mathcal{S}'_{p,m} - \mathcal{S}'_{p,q} \right\|_{MT}\right), & \text{otherwise} \end{cases} \end{aligned} \tag{6}$$

In this expression, $\|\cdot\|_M$ denotes the Manhattan distance. Note that $\|\cdot\|_{MT}$ actually represents the minimum inter-pixel distance via adjoining pixels, and it is different from the Manhattan distance. For example, as shown in Fig. 3a, the Manhattan distance from pixel A to B is 3 while the Manhattan distance-type distance is 5. Besides, if two pixels such as pixels B and C in Fig. 3a are not connected to

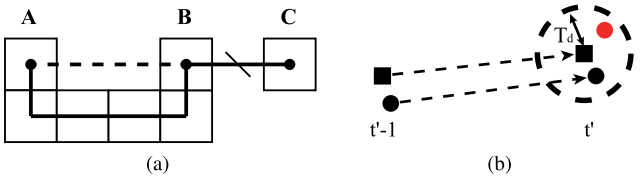

FIGURE 3. The illustrations of (a) distance measure in the segmentation step and (b) the framework of tracking. In (a), the dashed line and solid line respectively indicate the Manhattan distance and Manhattan distance-type distance. Besides, pixels B and C are not connected to each other via adjoining pixels. In (b), the circle and square respectively represent the observed and predicted clusters. clusters of different colors are different in terms of feature.

each other via adjoining pixels, the Manhattan distance-type distance is equal to infinity.

In order to extract each power-concentrated area, we just need to allocate adjoining pixels in the selected L' pixels to a segment. Each time we pick out the pixel with the strongest power from the rest of L' pixels. Then by taking the selected pixel as starting point and implementing Depth First Search (DFS) method [26], we can find all the pixels which are connected to that pixel. The selected-pixel-centric coarse-grained segment can be finally determined, and the pixels in the segment are removed from L' pixels. This repeated segmentation ends when no pixel from L' pixels remains. The coarse-grained segmentation result is shown in Fig. 2b.

3) FINE-GRAINED SEGMENTATION

MPCs in the channel always appear in distinct clusters which can be represented by segments in the power spectrum. However, clusters will be overlapped with each other if parameters of MPCs in these clusters are too close. That is to say, there are actually multiple clusters contained in a coarse-grained segment. For the further segmentation of these coarse-grained segments, we can implement the fuzzy c-means (FCM) algorithm [27]. According to the attenuated power distribution within clusters [28], the pixel whose power is stronger than that of neighbors (the definition of neighbor can be referred to in Eqs. (3)) in a coarse-grained segment can be regarded as the center of some cluster. Assume there are totally I_p pixels in the pth coarse-grained segment, and their location indices are respectively denoted as $\mathcal{S}'_{p,i}, i = 1, \ldots, I_p$. Besides, J_p cluster centers are detected in the coarse-grained segment, and their location indices are likewise denoted as $\mathcal{S}''_{p,j}, j = 1, \ldots, J_p$. Consequently, the objective function of FCM can be expressed as

$$Q = \sum_{i=1}^{I_p}\sum_{j=1}^{J_p} u_{ij}^r \exp\left(\left\|\mathcal{S}'_{p,i} - \mathcal{S}''_{p,j}\right\|_{MT}\right)$$
$$\text{s.t.} \sum_{j=1}^{J_p} u_{ij} = 1 \tag{7}$$

where $u_{ij} \in [0, 1]$ is the fuzzy membership which determines probability of the ith pixel belonging to the jth cluster and r is a membership coefficient which is generally taken as 2. It is noteworthy that the distance $\|\cdot\|_{MT}$ can be readily solved by Breadth First Search (BFS) method [26]. In addition, the construction of $e^{\|\cdot\|_{MT}}$ is based on the assumption of exponential decay law observed in [28]. Solve the optimization problem (7), and the membership can be obtained as

$$u_{ij} = \frac{1}{\sum_{k=1}^{J_p}\left(\frac{\exp\left(\left\|\mathcal{S}'_{p,i} - \mathcal{S}''_{p,j}\right\|_{MT}\right)}{\exp\left(\left\|\mathcal{S}'_{p,i} - \mathcal{S}''_{p,k}\right\|_{MT}\right)}\right)^{\frac{1}{r-1}}}. \tag{8}$$

The membership should be reset to 0 when $u_{ij} < \frac{1}{J_p}$. It means we can think that the ith pixel doesn't belong to the jth cluster when the membership is relatively low. Then we need to renormalize the membership as $\widetilde{u}_{ij} = \frac{u_{ij}}{\sum_{j=1}^{J_p} u_{ij}}$, and finally clusters in the coarse-grained segment are separated. Differing from the conventional clustering, one pixel may belong to multiple clusters with a certain membership in our result. The example of fine-grained segmentation result is shown in Fig. 2c.

B. FRAMEWORK OF TRACKING

The change between consecutive snapshots is insignificant by taking into account that the snapshot observation interval is generally short. Thus we can guarantee that the location and power distribution of the tracked cluster in the power spectrum change slightly. Based on this premise, the framework of tracking is divided into two stages, i.e., candidate search and feature matching.

1) CANDIDATE SEARCH

Suppose the observed mean, or rather, fuzzy power weighted nominal delay and Doppler frequency of the jth cluster in the pth coarse-grained segment at the current snapshot t' are denoted as $\widetilde{\boldsymbol{\mu}}_{t'} = [\widetilde{\tau}_{t'}, \widetilde{\nu}_{t'}]^{\mathrm{T}}$. It can be derived from the power spectrum as follows,

$$\widetilde{\boldsymbol{\mu}}_{t'} = \begin{bmatrix}\tau_{\lfloor\widetilde{m}\rfloor}\\ \nu_{\lfloor\widetilde{n}\rfloor}\end{bmatrix} + \begin{bmatrix}\widetilde{m} - \lfloor\widetilde{m}\rfloor\\ \widetilde{n} - \lfloor\widetilde{n}\rfloor\end{bmatrix} \odot \begin{bmatrix}\tau_{\lfloor\widetilde{m}\rfloor+1} - \tau_{\lfloor\widetilde{m}\rfloor}\\ \nu_{\lfloor\widetilde{n}\rfloor+1} - \nu_{\lfloor\widetilde{n}\rfloor}\end{bmatrix} \tag{9}$$

where $\odot$ and $\lfloor\cdot\rfloor$ are respectively Hadamard product and floor function. Besides, the subpixel level column index $\widetilde{m}$ and row index $\widetilde{n}$, which leads to super-resolution estimation of delay and Doppler compared with the sample interval, can be obtained as

$$\begin{bmatrix}\widetilde{m}\\ \widetilde{n}\end{bmatrix} = \sum_{i=1}^{I_p} \frac{u_{ij}P_i}{\sum_{k=1}^{I_p} u_{kj}P_k}\begin{bmatrix}m_i\\ n_i\end{bmatrix} \tag{10}$$

where u_{ij}, P_i, m_i, n_i are respectively the fuzzy membership, power density, column and row index of the ith pixel in the pth coarse-grained segment. In general, we directly use the system resolution as the sample interval, and Eq. (9) are simplified as

$$\widetilde{\boldsymbol{\mu}}_{t'} = \sum_{i=1}^{I_p} \frac{u_{ij}P_i}{\sum_{k=1}^{I_p} u_{kj}P_k}\begin{bmatrix}m_i\tau'\\ n_i\nu'\end{bmatrix} \tag{11}$$

where τ' and ν' are respectively the system resolution of delay and Doppler frequency.

Suppose the intrinsic parameter set of the cluster in the current snapshot t' is $\Theta_{t'} = [\tau_{t'}, \Delta\tau_{t'}, \nu_{t'}, \Delta\nu_{t'}]^{\mathrm{T}}$ where $\tau_{t'}$ and $\nu_{t'}$ are delay and Doppler free of noise. Moreover, $\Delta\tau_{t'}$ and $\Delta\nu_{t'}$ are rates of change for delay and Doppler. Then, the state-space model and observation model for the cluster are respectively formulated as

$$\Theta_{t'} = \mathbf{A}\Theta_{t'-1} + \mathbf{w}_{t'} \tag{12}$$

and

$$\widetilde{\boldsymbol{\mu}}_{t'} = \mathbf{H}\Theta_{t'} + \mathbf{v}_{t'} \tag{13}$$

where $\mathbf{w}_{t'}$ and $\mathbf{v}_{t'}$ are process noises and measurement noises in the current snapshot t', and covariance matrices of them are denoted as $\mathbf{Q}$ and $\mathbf{R}$. Besides,

$$\mathbf{A} = \begin{bmatrix} 1 & 1 & 0 & 0 \\ 0 & 1 & 0 & 0 \\ 0 & 0 & 1 & 1 \\ 0 & 0 & 0 & 1 \end{bmatrix}$$

and

$$\mathbf{H} = \begin{bmatrix} 1 & 0 & 0 & 0 \\ 0 & 0 & 1 & 0 \end{bmatrix}$$

are respectively state transition matrix and measurement matrix. According to the derivation of Kalman filter [29], the prediction step for parameter tracking is formulated as

$$\Theta_{t'|t'-1} = \mathbf{A}\Theta_{t'-1|t'-1} \tag{14}$$

$$\mathbf{P}_{t'|t'-1} = \mathbf{A}\mathbf{P}_{t'-1|t'-1}\mathbf{A}^{\mathrm{T}} + \mathbf{Q} \tag{15}$$

where $t'|t'-1$ denotes prediction of cluster states Θ and estimation error covariance $\mathbf{P}$ given information of the previous snapshot and $t'|t'$ denotes update of states and estimation error covariance based on the information of the current snapshot. Note that when the cluster in the previous snapshot (called as previous cluster for brevity hereinafter) is new, we can skip the step of feature matching and directly track the cluster in current snapshot by the minimum parameter difference. Then, to track the cluster in the next snapshot, the error covariance matrix $\mathbf{P}$ in the current snapshot can be initialized as $\mathbf{0}$ and parameters $\tau_{t'}$ and $\nu_{t'}$ are respectively initialized by observed parameters of the cluster $\widetilde{\tau}_{t'}$ and $\widetilde{\nu}_{t'}$. Moreover, parameters $\Delta\tau_{t'}$ and $\Delta\nu_{t'}$ are initialized by the difference of delay and Doppler between the current and previous snapshots. When the previous cluster is not new, we should implement the prediction step of Kalman filter using Eqs. (14) and (15). If the pixel-level distance between observed and predicted nominal parameters satisfies $\sqrt{\left(\frac{\tau_{t'|t'-1}-\widetilde{\tau}_{t'}}{\tau'}\right)^2 + \left(\frac{\nu_{t'|t'-1}-\widetilde{\nu}_{t'}}{\nu'}\right)^2} < T_d$ where T_d is a predefined threshold of pixel-level distance, the corresponding observed cluster in the power spectrum can be regarded as one of the candidate consequent clusters. For example, as shown in Fig. 3b, there are two observed clusters whose distances from the predicted cluster are lower than T_d, and therefore they are both candidate consequent clusters for the previous cluster.

2) FEATURE MATCHING

We propose a gradient-based histogram of power (GBHOP) method which learns from the idea of histogram of gradient (HOG) [30] to describe the feature of each cluster. Briefly speaking, powers and gradient moduli of pixels respectively serve as elements of the abscissa and ordinate in the histogram. Considering that the span of powers in the spectrum is large enough and power levels of clusters are generally different, powers are appropriate to be divided into bins. Suppose the maximum number of pixels in one cluster is Y. According to Sturges' formula [31], the number of bins g can be reasonably determined as

$$g = 1 + 3.322\lg Y. \tag{16}$$

Consequently, the bin size is set as $d = \frac{P_{\max}}{g}$ assuming the maximum power of pixels in the power spectrum is equal to $P_{\max}$. Differing from the conventional occurrence frequency based histogram, in our method, gradient moduli of pixels are accumulated in the corresponding bin. The gradient modulus of the pixel with location index (m, n) reads

$$|G(m,n)| = \sqrt{\left(\frac{P(m,n+1)-P(m,n-1)}{2}\right)^2 + \left(\frac{P(m-1,n)-P(m+1,n)}{2}\right)^2}. \tag{17}$$

Gradient modulus distributions with respect to power are different for each cluster, and therefore GBHOP can be used to distinguish different clusters.

Assume histograms of the previous cluster and one of the candidate consequent clusters in current snapshot which is predicted in the candidate search step are respectively vectorized as $\boldsymbol{h}_1$ and $\boldsymbol{h}_2$. Then the similarity between the two clusters can be quantified by cosine similarity [32], i.e.,

$$\mathrm{sim}(\boldsymbol{h}_1, \boldsymbol{h}_2) = \frac{\boldsymbol{h}_1 \cdot \boldsymbol{h}_2}{\|\boldsymbol{h}_1\| \, \|\boldsymbol{h}_2\|}. \tag{18}$$

When $\mathrm{sim}(\boldsymbol{h}_1, \boldsymbol{h}_2) \geq T_s$ where T_s is a predefined threshold of cosine similarity which is generally set to 0.5 [33], we consider that the candidate cluster is evolution of the previous cluster, such as the candidate cluster that is the same color as the previous observed cluster in Fig. 3b. Suppose the observed parameters of the candidate cluster are $\widetilde{\boldsymbol{\mu}}_{t'}$, and then they are used in the second step of Kalman filter for parameter update as follows,

$$\mathbf{K} = \mathbf{P}_{t'|t'-1}\mathbf{H}\left(\mathbf{H}\mathbf{P}_{t'|t'-1}\mathbf{H}^{\mathrm{T}} + \mathbf{R}\right)^{-1} \tag{19}$$

$$\Theta_{t'|t'} = \Theta_{t'|t'-1} + \mathbf{K}\left(\widetilde{\boldsymbol{\mu}}_{t'} - \mathbf{H}\Theta_{t'|t'-1}\right) \tag{20}$$

$$\mathbf{P}_{t'|t'} = (\mathbf{I} - \mathbf{K}\mathbf{H})\,\mathbf{P}_{t'|t'-1} \tag{21}$$

where $\mathbf{I}$ is identity matrix and $\mathbf{K}$ is the Kalman gain. Based on the observed values, predicted values and Kalman gain, cluster states Θ and estimation error covariance $\mathbf{P}$ are

updated respectively in Eqs. (20) and (21). Subsequently, these updated parameters can serve as the previous information to iteratively search for candidate consequent clusters in the next snapshot following Eqs. (14) and (15) in the step of candidate search. The Kalman filter is used for each cluster in the previous snapshot, and finally the evolution of these clusters can be all determined through the steps of candidate search and feature matching. It is noteworthy that if there is feature mismatch between some candidate cluster and any of its previous clusters, the candidate cluster is deemed as a new cluster. Moreover, if there is mismatch between some previous cluster and any of its candidate clusters, the previous cluster is considered to disappear.

Additionally, there are two points to note. For one thing, due to the multipath fading and measurement noises, some clusters in a few snapshots may disappear which leads to the tracking interruption. In order to successfully track clusters, for clusters which are deemed as new clusters in the current snapshot, we can use a 'retrospect' way to find their origins in earlier snapshots skipping the previous snapshot. For another, besides cluster birth and death, another three evolution modes may appear in the process of cluster tracking as shown in Figs. 4. The first is splitting which occurs when multiple candidate consequent clusters are found, and they all match to the common previous cluster. The second is fusing. It occurs when multiple previous clusters evolve to the common candidate consequent cluster. The cluster is then deemed as a new cluster. As for the last situation, it is a mixture of the former two situations. That is to say, one previous cluster splits into multiple consequent clusters, and some of the consequent clusters fuse with clusters which evolve from other previous clusters to form new clusters.

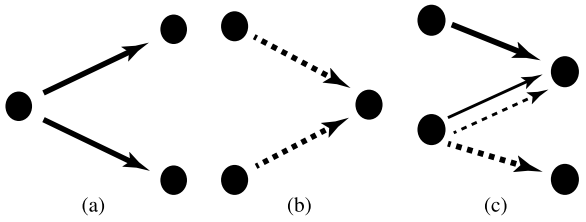

FIGURE 4. Diagrams of three cluster evolution modes: (a) splitting, (b) fusing and (c) mixture of splitting and fusing. The solid line represents the process of splitting and the dashed line represents fusing. Besides, dots on the left and right are clusters respectively in the previous and current snapshot.

III. SIMULATION STUDIES

In this section, we carry out a synthetic channel simulation in a predetermined dynamic scenario to evaluate performance of the proposed tracker.

A. SCENARIO SETTING

The simulation is designed based on the stochastic propagation graph theory and the detailed simulation procedure can be referred to in [34]. For simplicity, we only consider the planar situation and single-input-single-output (SISO) antenna system. The illustration conceived for the channel simulation is shown in Fig. 5. As for settings of the simulation, the transmitter (Tx) locates at the origin and the receiver (Rx) is moving towards the Tx at a speed of 60 km/h from 50 m away. Except for the direct propagation path from the Tx to Rx, there are two fixed objects on both sides of the moving Rx as illustrated in the figure and they additionally lead to ray scattering. In order to focus the scattered rays on a cluster, we need to guarantee that the length of objects is small enough, e.g., 10 cm adopted in our graph simulation. In addition, other necessary parameters for the simulation are listed in Table 1.

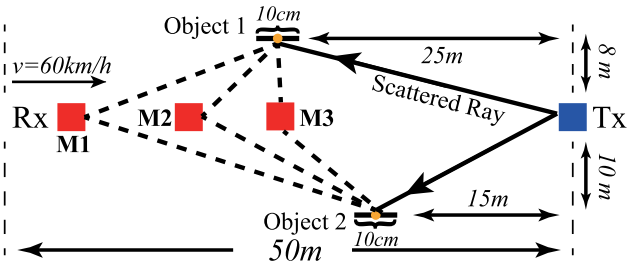

FIGURE 5. The scenario illustration for channel simulation. The Tx, Rx and two objects are labeled. The Rx will receive rays coming from scattering points which are represented by orange dots. As the Rx moves towards the Tx, it passes by three positions which are marked as M1, M2 and M3. The cluster evolution mode of M1 to M2 is fusing and M2 to M3 is splitting.

TABLE 1. Parameters for synthetic channel simulation.

Parameters	Values
Center Frequency	6 GHz
Bandwidth	500 MHz
Signal to Noise Ratio (SNR)	30 dB
Number of Frequency Points	2048
Number of Scattering Points in Each Object	20
Duration of One Cycle	1 ms
Number of Cycles in One Snapshot	20
Number of Snapshots	2000
Number of Candidate Pixels L	80
Threshold of pixel-level distance T_d	0.5
Threshold of Cosine Similarity T_s	0.5

We assume that a few scattering points are randomly distributed on the two objects for each cycle which is defined as the duration of one channel measurement. Note that in the simulation we suppose that only single-bounce scattering happens. As the Rx moves towards the Tx, two evolution modes of clusters, namely fusing and splitting coherently exist. The evolution modes have been described in Section II, and we will demonstrate them through the simulation results in the next subsection. It is noted that the duration of 20 cycles is lower than coherence time that is around 24.5 ms based on the Doppler spread in the first cycle, which indicates that the assumption of WSSUS basically holds in each snapshot. Hence, the temporal-frequency channel coefficient for each snapshot that contains 20 cycles is calculated using

the propagation graph theory and it is then transformed to delay-Doppler power spectrum using Eq. (1) for further application of the tracker and evaluation of the simulation.

B. EVALUATION RESULTS

Figs. 6 sequentially display the cluster tracking results in snapshot 650, 1150 and 1450 to demonstrate cluster evolution during the simulation, and they respectively correspond to the positions M1, M2 and M3 marked in Fig. 5. At first, there are three separate clusters in which the earliest cluster results from the direct path between the Tx and Rx, and the other two clusters are caused by rays scattered from the two objects. As shown in Fig. 6a, Doppler frequencies of the three clusters are all positive since the Rx is moving towards the Tx and two objects. As the Rx approaches the Tx, delays of these clusters become smaller. The clusters from the two objects also approach each other, and ultimately they are integrated into a new cluster. As for the third stage, the combined cluster is separated again. However, the clusters caused by reflections become inconspicuous in the contour plot because the power of direct path is so strong that leads to the large power difference between the direct path and reflected paths. Under the circumstances, we can still track these clusters and determine their nominal centers and spreads. According to Fig. 5, Doppler frequencies of the paths from Object 1 become around zero and it coincides with the result in Fig. 6c.

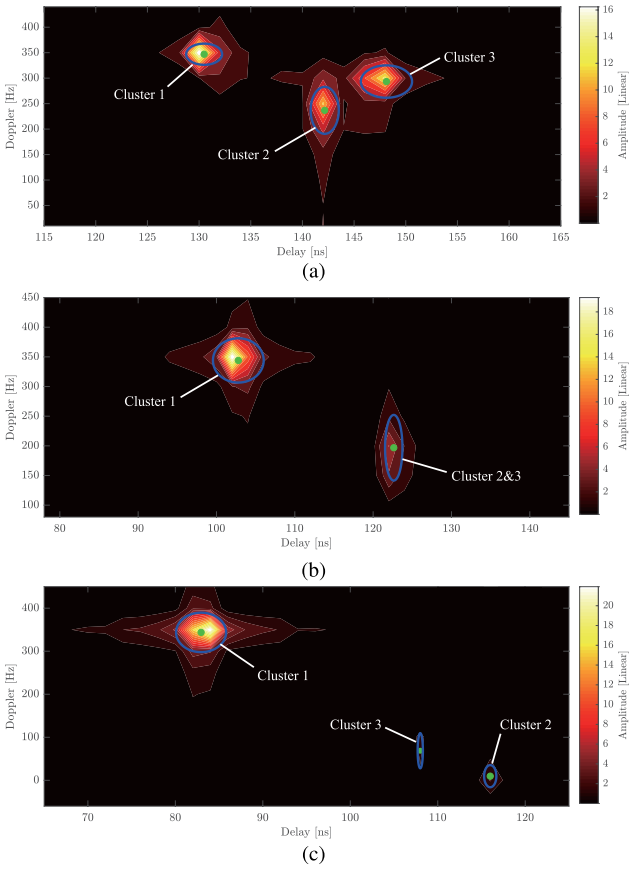

FIGURE 6. The demonstration of three positions in the simulation: (a) M1, (b) M2 and (c) M3. The green dot indicates power weighted nominal delay and Doppler, and the blue ellipse shows both the delay spread and Doppler spread.

In view of the power weighted nominal delay and Doppler which are formulated as Eq. (11), fuzzy power weighted delay spread $\widetilde{\sigma}_{\tau,t'}$ and Doppler spread $\widetilde{\sigma}_{\nu,t'}$ of the jth cluster in the pth coarse-grained segment at the current snapshot t' can be similarly predicted as

$$\begin{bmatrix}\widetilde{\sigma}_{\tau,t'}\\ \widetilde{\sigma}_{\nu,t'}\end{bmatrix}=\sqrt{\sum_{i=1}^{I_p}\frac{u_{ij}P_i}{\sum_{k=1}^{I_p}u_{kj}P_k}\left(\begin{bmatrix}m_i^2\\ l_i^2\end{bmatrix}\odot\begin{bmatrix}\tau'^2\\ \nu'^2\end{bmatrix}\right)-\begin{bmatrix}\widetilde{\tau}_{t'}^2\\ \widetilde{\nu}_{t'}^2\end{bmatrix}} \quad (22)$$

when we simply adopt the system resolution as the sample interval. It is clear that the tracked nominal delay and Doppler values which are represented by dots coincide with centers of clusters (power-concentrated areas) in the power spectrum. Moreover, the predicted spreads which are represented by ellipses almost overlap the boundary of clusters. These results manifest the effectiveness of the proposed tracker. It is noteworthy that the range of delay and Doppler spread is a little smaller than the boundary of clusters due to the rigourous pixel selection in the image denoising step where only the pixels with strong power remain.

Figs. 7 show the comparison among theoretical values (mean delay and Doppler calculated from the simulation) and tracked values respectively from the proposed PSBST, the PASCT [24] and the conventional KPMCT [8] from snapshot 680 to 780 when three clusters coexist. As regards the KPMCT, we use the combination of Calinski-Harabasz index (CH) and Davies-Bouldin index (DB) [35] to automatically determine the number of clusters and then iteratively run the KPowerMeans algorithm with the definite number of clusters five times to guarantee the clustering convergence. Finally, the MCD of each pair of clusters is used to track clusters. As for the PASCT, we set the number of power levels as 20 to extract objects from the background with the between-class-variance rule. Besides, we respectively set the weight coefficients of three characteristics as 1, 5 and 1 to measure the distance between clusters and use Kuhn-Munkres (K-M) approach to track clusters based on the distance. Note that the tracked results from KPMCT seem smoother than those from PSBST and PASCT because power spectrum based trackers are more affected by the multipath fading in clusters. However, outliers which don't belong to any specific cluster sometimes appear because KPMCT is unable to separate clusters when multipaths from these clusters are concentrated. In contrast, PSBST and PASCT can both separate these adjacent clusters and track the clusters the whole time. Furthermore, we calculate average root mean square errors of estimation (RMSEEs) between tracked values and theoretical values from 150 simulations for both delay and Doppler. RMSEEs of each cluster and total clusters are listed in Table 2. In general, the accuracy of PSBST is slightly inferior to that of KPMCT which is based on the SAGE algorithm with high-resolution and it is close to the accuracy

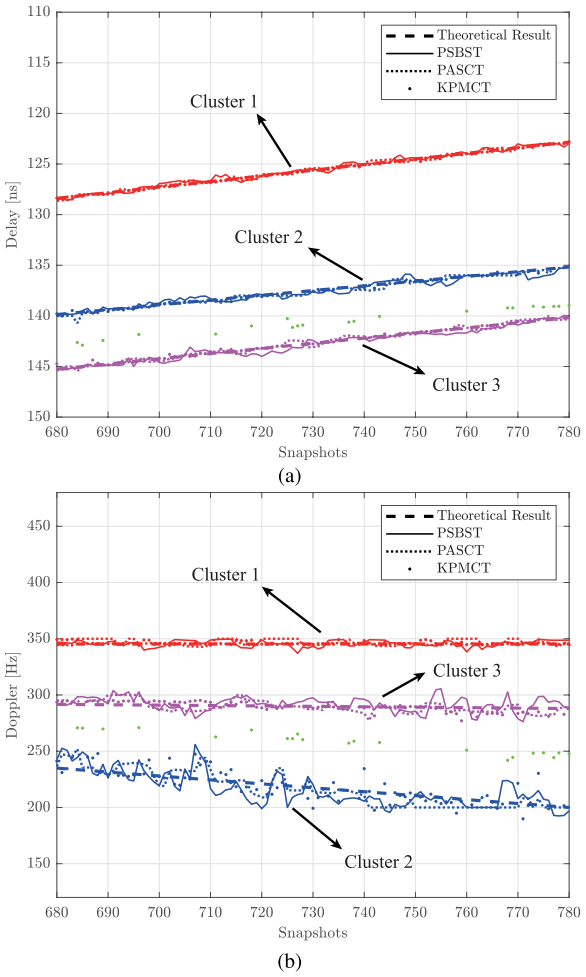

FIGURE 7. The comparisons between theoretical and tracked values with respect to (a) delay and (b) Doppler in 101 snapshots. The green dots are outliers from KPMCT and don't belong to any specific cluster.

TABLE 2. The comparison of RMSEEs among KPMCT, PASCT and PSBST.

	RMSEEs of Delay [ns]			RMSEEs of Doppler [Hz]		
	KPMCT	PASCT	PSBST	KPMCT	PASCT	PSBST
Cluster 1	0.06	0.20	0.22	1.49	2.88	2.83
Cluster 2	0.27	0.33	0.34	9.56	9.62	10.16
Cluster 3	0.29	0.32	0.32	3.69	7.81	6.31
Total	0.20	0.28	0.29	4.69	6.77	6.43

of PASCT. Moreover, the RMSEE of PSBST is much less than the system resolution which is 2 ns in delay domain and 50 Hz in Doppler domain. It can well satisfy the practical application. In fact, RMSEE of the proposed tracker generally depends on the applied system resolution, and high resolution brings about great accuracy.

As for the computational speed, we compare the running time of PSBST, PASCT and KPMCT in both the simulation and measurement which is presented in Section IV. Considering that the running time varies in different snapshots because of the time-variant channel, we adopt the average running time of each snapshot as a metric for the computational speed. The average running time is listed in Table 3. The results

TABLE 3. The comparison of computational speed among PSBST, PASCT and KPMCT.

	PSBST	PASCT	KPMCT
Simulation	0.04 s	0.12 s	62.43 s
Measurement	0.37 s	0.76 s	205.59 s

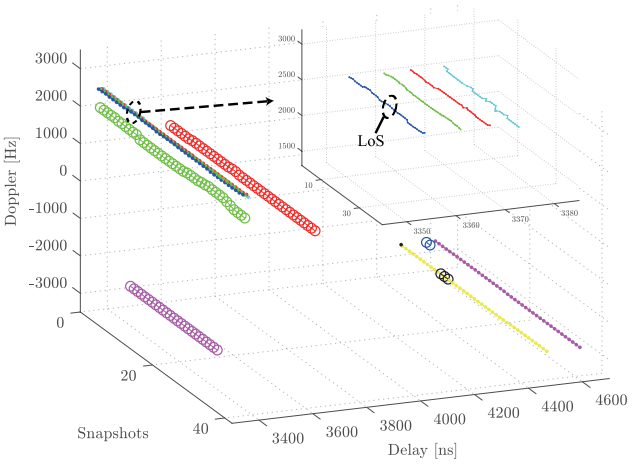

FIGURE 8. The result of cluster tracking in the V2X scenario. Different colors and marker shapes represent different tracks. The subfigure which is pointed by the dotted arrow shows the enlarged details of entangled tracks marked by dashed circle.

demonstrate that the KPMCT needs the most time due to the high-resolution channel parameter estimation. Additionally, the PSBST is a little faster than the PASCT because it simplifies the procedure of cluster extraction from power spectrum compared with PASCT. In conclusion, our proposed tracker can identify and track clusters with satisfactory accuracy and less computational time.

IV. APPLICATION IN V2X TIME-VARIANT CHANNEL

A field measurement has been conducted in an inter-state expressway in Yeoju, South Korea. As for the measurement setup, a SISO channel sounder is used to collect data. The Tx directional antenna is fixed on a bridge in the expressway and the Rx omnidirectional antenna is installed on the roof of a car which moves towards the transmitter at the speed of around 100 km/h. The center frequency of the transmitted signal is 28 GHz and the bandwidth of the signal is 500 MHz which leads to the delay resolution of 2 ns. In addition, the observation interval of signal is approximately 0.066 ms. It implies that the Doppler frequency range we can obtain is around -7630 Hz to 7630 Hz according to Eq. (1). It is noted that there is infrastructure and passing vehicles in the expressway, and therefore it is a typical time-variant V2X scenario. The detailed description including measurement setup and environment is referred to in [36].

In order to verify the applicability of the proposed PSBST, we apply the tracker to track clusters in the V2X time-variant channel based on the collected data. We regard 110 continuous cycles as a snapshot, and hence the resolution of Doppler

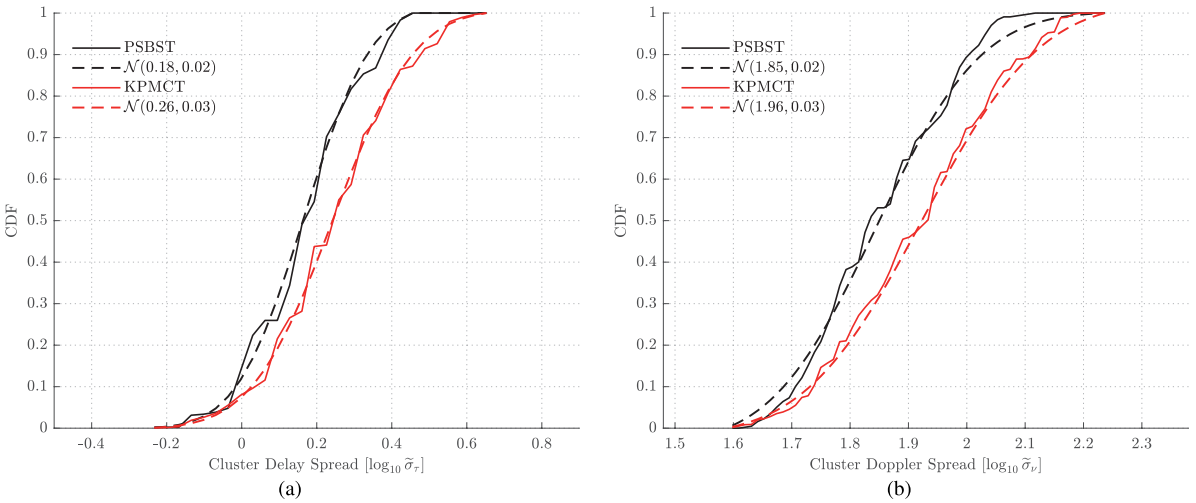

FIGURE 9. Statistical characteristics for intra-cluster parameters (a) cluster delay spread in common logarithm and (b) cluster Doppler spread in common logarithm. The solid lines represent empirical CDFs and dashed lines represent fitted CDFs.

frequency is around 138 Hz which is much lower than thousands of Hertz existing in the environment of expressway. Additionally, the number of candidate pixels L, threshold of pixel-level distance T_d and threshold of cosine similarity T_s are respectively set to 2035, 0.5 and 0.5 for the application.

The result of cluster tracking is shown in Fig. 8. Several distinct trajectories appear in the time-variant channel, and most of them last for a long period of time. It is noteworthy that the clusters which are close to each other are obviously separated using the proposed tracker as shown in the subfigure of Fig. 8. Furthermore, the states of these trajectories are consistent with the measurement environment description mentioned in [36]. For example, delay of the cluster which results from the LOS (Line-of-Sight) path decreases with time and its Doppler frequency remains at around 2600 Hz because the Rx approaches Tx at the speed of 100 km/h. The other three clusters in the subfigure whose Doppler is close to 2600 Hz and propagation distances are at most 6 m longer than the LOS cluster may be generated by infrastructure along the roadside and nearby passing vehicles. Moreover, the clusters with larger delay and negative Doppler are generated by reflective paths from the overpass and distant buildings behind the Rx. Obviously, PSBST is able to effectively detect and track clusters in the time-variant channel. It also provides a good match between the tracked clusters and objects in the measurement environment.

In addition, we can preliminarily analyze the statistical characteristics for intra-cluster and inter-cluster parameters based on the proposed PSBST. These parameters contribute to the construction of cluster-based time-variant channel models, e.g., random-cluster channel model [5] and COST 2100 channel model [6] for V2X scenario. As for the intra-cluster parameters, we pay attention to the root mean square (RMS) cluster delay spread and Doppler spread of tracked clusters. These parameters can be readily obtained according to Eq. (22). Figs. 9 depict the appropriate CDFs

TABLE 4. Parameters of fitted CDFs for intra-cluster and inter-cluster parameters.

	Cluster Delay Spread [ns]		Cluster Doppler Spread [Hz]		LOS Power Factor [dB]	
	KPMCT	PSBST	KPMCT	PSBST	KPMCT	PSBST
Distribution	Lognormal	Lognormal	Lognormal	Lognormal	Normal	Normal
μ	0.26	0.18	1.96	1.85	-3.53	-1.17
σ^2	0.03	0.02	0.03	0.02	7.42	6.87
Mean	1.97	1.60	98.75	74.65	-3.53	-1.17
STD	0.82	0.53	41.00	24.97	2.72	2.62

for these two kinds of cluster spreads which are in the form of common logarithm. In order to verify the rationality of statistical characteristics derived from PSBST, we compare the results with those from KPMCT which is commonly used in cluster-based time-variant channel modeling. The appropriate CDFs for the cluster spreads from KPMCT are also shown in Figs. 9. The details of intra-cluster parameters from PSBST and KPMCT are listed in Table 4. It can be observed that the fitted CDF of PSBST is close to that of KPMCT. Note that the mean values derived from PSBST is a little smaller than those derived from KPMCT because of the rigourous pixel selection in the image denoising step which narrows down the range of clusters. Besides, the obtained distribution functions of cluster delay spread and Doppler spread are the same as those mentioned in [37] although the parameters of distribution functions are different due to different environments and frequency bands. Combined with the cluster tracking shown in Fig. 8, we find the clusters are sparse but energy-concentrated in the expressway fast fading channel.

We also investigate the statistical characteristics for LOS power factor which is an inter-cluster parameter mentioned in the COST 2100 channel model. The LOS power factor is defined as power ratio of the first arriving MPC and other MPCs. Because of the pixel-level power resolution in PSBST,

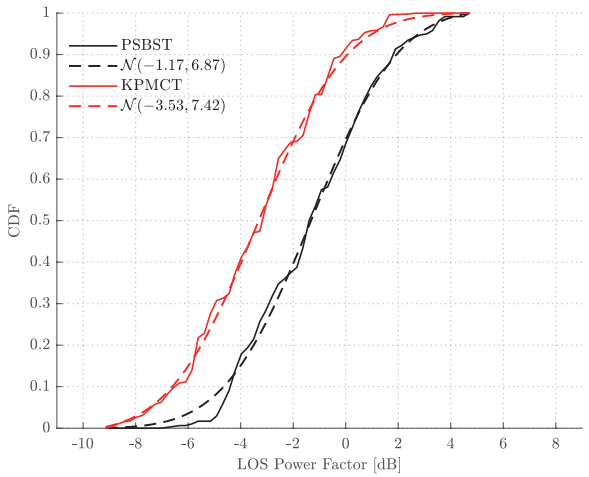

FIGURE 10. Statistical characteristics for the inter-cluster parameter LOS K-factor. The solid lines represent empirical CDFs and dashed lines represent fitted CDFs.

we can roughly estimate the LOS power factor as

$$K_{\mathrm{LOS}} = 10\log_{10}\frac{P_{\max}}{P_{\mathrm{tot}} - P_{\max}} \tag{23}$$

where P_{tot} is the total sum of powers of L' pixels which are finally selected in the image denoising step. Fig. 10 shows the appropriate CDFs for LOS power factors derived from PSBST and KPMCT. The details of LOS power factor statistical characteristics are also listed in Table 4. It can be observed that the mean LOS power factor from PSBST is a little larger than that from KPMCT due to the inseparability of LOS power in PSBST. Note that the obtained mean value and standard deviation are close to those mentioned in [38]. Considering that the Tx is relatively far away from the Rx in our measurement, the power of LOS path is prominent which leads to the higher LOS power factor compared with that from [38].

These statistical distributions derived from PSBST can be further used to simulate the V2X channel combined with cluster-based channel models. In a word, PSBST is a useful tool which can not only dynamically reproduce the nonstationary time-variant channel in conformity with the actual environment, but also rapidly and reasonably accomplish the cluster-based channel modeling for a specific scenario compared with the conventional parameter estimation based cluster tracking method.

V. CONCLUSION

In the paper, we present a novel power spectrum based cluster tracking method PSBST to analyze the characteristics of time-variant channel. The tracker can distinguish overlapped clusters in the power spectrum through three stages, namely image denoising, coarse-grained segmentation and fine-grained segmentation. Then clusters in consecutive snapshots can be sequentially tracked based on the combination of Kalman filter and GBHOP methods. The synthetic channel simulation shows that the tracker can reach low estimation errors and its average running time is less than that of existing cluster tracking algorithms. Additionally, the application in time-variant V2X channel demonstrates that PSBST can accurately reproduce the cluster evolution. It also contributes to cluster-based channel modeling by reasonably extracting the cluster statistical characteristics, e.g., intra-cluster and inter-cluster parameters, from tracking results.

We take the SISO channel as an example in this article. In fact, our proposed tracker is also applicable to the MIMO channel. For one thing, we can use multiple PSBSTs to cooperatively process multiple power spectrums from receivers and accomplish cluster tracking combined with these processed results. For another, we can apply the tracker to more spectrums besides the delay-Doppler power spectrum. For instance, we can apply the PSBST to the power-angle spectrum as long as we obtain the spectrum from the conventional Bartlett beamformer [39]. In the follow-up work, we will apply the tracker to time-variant MIMO channel for the study of spatial or higher-dimensional channel characteristics.

ACKNOWLEDGMENT

The authors would like to thank Jae-Joon Park and Myung-Don Kim, Electronics and Telecommunications Research Institute (ETRI) for conducting the field measurement and providing the measurement data.

REFERENCES

[1] N. Czink, X. Yin, H. Ozcelik, M. Herdin, E. Bonek, and B. Fleury, "Cluster characteristics in a MIMO indoor propagation environment," *IEEE Trans. Wireless Commun.*, vol. 6, no. 4, pp. 1465–1475, Apr. 2007.

[2] S. L. H. Nguyen, K. Haneda, and J. Putkonen, "Dual-band multipath cluster analysis of small-cell backhaul channels in an urban street environment," in *Proc. IEEE Globecom Workshops (GC Wkshps)*, Dec. 2016, pp. 1–6.

[3] C. Ling, X. Yin, R. Müller, S. Häfner, D. Dupleich, C. Schneider, J. Luo, H. Yan, and R. Thomä, "Double-directional dual-polarimetric cluster-based characterization of 70–77 GHz indoor channels," *IEEE Trans. Antennas Propag.*, vol. 66, no. 2, pp. 857–870, Feb. 2018.

[4] A. A. M. Saleh and R. Valenzuela, "A statistical model for indoor multipath propagation," *IEEE J. Sel. Areas Commun.*, vol. 5, no. 2, pp. 128–137, Feb. 1987.

[5] N. Czink, E. Bonek, L. Hentila, J.-P. Nuutinen, and J. Ylitalo, "A measurement-based random-cluster MIMO channel model," in *Proc. IEEE Antennas Propag. Soc. Int. Symp.*, Jun. 2007, pp. 5363–5366.

[6] L. Liu, C. Oestges, J. Poutanen, K. Haneda, P. Vainikainen, F. Quitin, F. Tufvesson, and P. Doncker, "The COST 2100 MIMO channel model," *IEEE Wireless Commun.*, vol. 19, no. 6, pp. 92–99, Dec. 2012.

[7] L. Vuokko, P. Vainikainen, and J. Takada, "Clusterization of measured direction-of-arrival data in an urban macrocellular environment," in *Proc. 14th IEEE Proc. Pers., Indoor Mobile Radio Commun. (PIMRC)*, vol. 2, Sep. 2003, pp. 1222–1226.

[8] N. Czink and C. Mecklenbrauker, "A novel automatic cluster tracking algorithm," in *Proc. IEEE 17th Int. Symp. Pers., Indoor Mobile Radio Commun.*, Sep. 2006, pp. 1–5.

[9] B. H. Fleury, M. Tschudin, R. Heddergott, D. Dahlhaus, and K. I. Pedersen, "Channel parameter estimation in mobile radio environments using the SAGE algorithm," *IEEE J. Sel. Areas Commun.*, vol. 17, no. 3, pp. 434–450, Mar. 1999.

[10] C.-X. Wang, X. Cheng, and D. Laurenson, "Vehicle-to-vehicle channel modeling and measurements: Recent advances and future challenges," *IEEE Commun. Mag.*, vol. 47, no. 11, pp. 96–103, Nov. 2009.

[11] A. Ghazal, C.-X. Wang, B. Ai, D. Yuan, and H. Haas, "A nonstationary wideband MIMO channel model for high-mobility intelligent transportation systems," *IEEE Trans. Intell. Transp. Syst.*, vol. 16, no. 2, pp. 885–897, Apr. 2015.

[12] X. Yin, X. Cai, X. Cheng, J. Chen, and M. Tian, "Empirical geometry-based random-cluster model for High-Speed-Train channels in UMTS networks," *IEEE Trans. Intell. Transp. Syst.*, vol. 16, no. 5, pp. 2850–2861, Oct. 2015.
[13] Y. Liu, C.-X. Wang, J. Huang, J. Sun, and W. Zhang, "Novel 3-D non-stationary mmWave massive MIMO channel models for 5G high-speed train wireless communications," *IEEE Trans. Veh. Technol.*, vol. 68, no. 3, pp. 2077–2086, Mar. 2019.
[14] L. Frenkel and M. Feder, "Recursive expectation-maximization (EM) algorithms for time-varying parameters with applications to multiple target tracking," *IEEE Trans. Signal Process.*, vol. 47, no. 2, pp. 306–320, Feb. 1999.
[15] P.-J. Chung and J. F. Bohme, "Recursive EM and SAGE-inspired algorithms with application to DOA estimation," *IEEE Trans. Signal Process.*, vol. 53, no. 8, pp. 2664–2677, Aug. 2005.
[16] J. Salmi, A. Richter, and V. Koivunen, "Enhanced tracking of radio propagation path parameters using state-space modeling," in *Proc. 14th Eur. Signal Process. Conf*, Sep. 2006, pp. 1–5.
[17] X. Yin, G. Steinbock, G. E. Kirkelund, T. Pedersen, P. Blattnig, A. Jaquier, and B. H. Fleury, "Tracking of time-variant radio propagation paths using particle filtering," in *Proc. IEEE Int. Conf. Commun.*, May 2008, pp. 920–924.
[18] C. Huang, R. He, Z. Zhong, Y.-A. Geng, Q. Li, and Z. Zhong, "A novel tracking-based multipath component clustering algorithm," *IEEE Antennas Wireless Propag. Lett.*, vol. 16, pp. 2679–2683, 2017.
[19] N. Czink, R. Tian, S. Wyne, F. Tufvesson, J.-P. Nuutinen, J. Ylitalo, E. Bonek, and A. F. Molisch, "Tracking time-variant cluster parameters in MIMO channel measurements," in *Proc. 2nd Int. Conf. Commun. Netw. China*, Aug. 2007, pp. 1147–1151.
[20] C. Huang, R. He, Z. Zhong, B. Ai, and Z. Zhong, "Comparison of automatic tracking and clustering algorithms for time-variant multipath components," in *Proc. IEEE Globecom Workshops (GC Wkshps)*, Dec. 2017, pp. 1–6.
[21] J. Gedschold, C. Schneider, M. Kaske, R. S. Thoma, G. Del Galdo, M. Boban, and J. Luo, "Tracking based multipath clustering in vehicle-to-infrastructure channels," in *Proc. IEEE 29th Annu. Int. Symp. Pers., Indoor Mobile Radio Commun. (PIMRC)*, Sep. 2018, pp. 1–5.
[22] F. Luan, A. F. Molisch, L. Xiao, F. Tufvesson, and S. Zhou, "Geometrical cluster-based scatterer detection method with the movement of mobile terminal," in *Proc. IEEE 81st Veh. Technol. Conf. (VTC Spring)*, May 2015, pp. 1–6.
[23] C. Huang, A. F. Molisch, Y.-A. Geng, R. He, B. Ai, and Z. Zhong, "Trajectory-joint clustering algorithm for time-varying channel modeling," *IEEE Trans. Veh. Technol.*, vol. 69, no. 1, pp. 1041–1045, Jan. 2020.
[24] C. Huang, R. He, Z. Zhong, B. Ai, Y.-A. Geng, Z. Zhong, Q. Li, K. Haneda, and C. Oestges, "A power-angle-spectrum based clustering and tracking algorithm for time-varying radio channels," *IEEE Trans. Veh. Technol.*, vol. 68, no. 1, pp. 291–305, Jan. 2019.
[25] P. Bello, "Characterization of randomly time-variant linear channels," *IEEE Trans. Commun.*, vol. 11, no. 4, pp. 360–393, Dec. 1963.
[26] T. H. Cormen, C. E. Leiserson, R. L. Rivest, and C. Stein, *Introduction to Algorithms*. Cambridge, MA, USA: MIT Press, 2009.
[27] J. C. Bezdek, R. Ehrlich, and W. Full, "FCM: The fuzzy C-means clustering algorithm," *Comput. Geosci.*, vol. 10, nos. 2–3, pp. 191–203, Jan. 1984.
[28] Q. H. Spencer, B. D. Jeffs, M. A. Jensen, and A. L. Swindlehurst, "Modeling the statistical time and angle of arrival characteristics of an indoor multipath channel," *IEEE J. Sel. Areas Commun.*, vol. 18, no. 3, pp. 347–360, Mar. 2000.
[29] R. G. Brown, *Introduction to Random Signal Analysis and Kalman Filtering*. New York, NY, USA: Wiley, 1983.
[30] N. Dalal and B. Triggs, "Histograms of oriented gradients for human detection," in *Proc. IEEE Comput. Soc. Conf. Comput. Vis. Pattern Recognit. (CVPR)*, vol. 1, Jun. 2005, pp. 886–893.
[31] H. A. Sturges, "The choice of a class interval," *J. Amer. Stat. Assoc.*, vol. 21, no. 153, pp. 65–66, Mar. 1926.
[32] A. Singhal, "Modern information retrieval: A brief overview," *IEEE Data Eng. Bull.*, vol. 24, no. 4, pp. 35–43, Dec. 2001.
[33] J. Cohen, *Statistical Power Analysis for the Behavioral Sciences*. Hillsdale, NJ, USA: Lawrence Earlbam Associates, 1988.
[34] L. Tian, X. Yin, Q. Zuo, J. Zhou, Z. Zhong, and S. X. Lu, "Channel modeling based on random propagation graphs for high speed railway scenarios," in *Proc. IEEE 23rd Int. Symp. Pers., Indoor Mobile Radio Commun. (PIMRC)*, Sep. 2012, pp. 1746–1750.
[35] N. Czink, P. Cera, J. Salo, E. Bonek, J.-P. Nuutinen, and J. Ylitalo, "A framework for automatic clustering of parametric MIMO channel data including path powers," in *Proc. IEEE Veh. Technol. Conf.*, Sep. 2006, pp. 1–5.
[36] J. Park, J. Lee, K. Kim, M. Kim, and K. C. Lee, "Multipath propagation characteristics for 5g vehicular communications based on 28 GHz expressway measurements," in *Proc. 13th Eur. Conf. Antennas Propag. (EuCAP)*, Mar. 2019, pp. 1–5.
[37] X. Cai, B. Peng, X. Yin, and A. P. Yuste, "Hough-transform-based cluster identification and modeling for V2V channels based on measurements," *IEEE Trans. Veh. Technol.*, vol. 67, no. 5, pp. 3838–3852, May 2018.
[38] Q. Wang, B. Ai, R. He, M. Yang, B. Zhang, J. Li, L. Chen, and X. Li, "Time-variant cluster-based channel modeling for V2V communications," in *Proc. IEEE Int. Conf. Commun. (ICC)*, May 2018, pp. 1–6.
[39] M. S. Babtlett, "Smoothing periodograms from time-series with continuous spectra," *Nature*, vol. 161, no. 4096, pp. 686–687, May 1948.

TIANQI WU (Graduate Student Member, IEEE) received the bachelor's degree in applied mathematics from the Zhejiang University of Technology, Hangzhou, Zhejiang, China, in 2018. He is currently pursuing the Ph.D. degree with the College of Electronics and Information Engineering, Tongji University, Shanghai, China. His research interests include time-variant channel modeling, high-resolution channel parameter estimation algorithm design, and 5G downlink channel characterization.

XUEFENG YIN (Member, IEEE) received the bachelor's degree in optoelectronics engineering from the Huazhong University of Science and Technology, Wuhan, China, in 1995, and the M.Sc. degree in digital communications and the Ph.D. degree in wireless communications from Aalborg University, Aalborg, Denmark, in 2002 and 2006, respectively. From 2006 to 2008, he was an Assistant Professor with Aalborg University. In 2008, he joined the College of Electronics and Information Engineering, Tongji University, Shanghai, China. He became a Full Professor, in 2016, and has been the Vice Dean of the college, since 2016. He has authored or coauthored more than 130 technical articles, four books, and 12 PCT patents. His research interests include high-resolution parameter estimation for propagation channels, measurement-based channel characterization, random propagation-graph-based channel simulations, radar signal processing, and target recognition assisted with deep learning techniques.

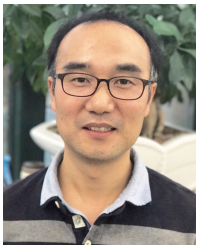

JUYUL LEE (Senior Member, IEEE) received the Ph.D. degree in electrical engineering from the University of Minnesota at Twin Cities, USA, in 2010. He was with the Agency for Defense Development, South Korea, from 1998 to 2000. Since 2000, he has been with the Electronics and Telecommunications Research Institute, South Korea, where he is currently a Principal Researcher with the Telecommunications and Media Research Laboratory. His current research interests include wireless channel modeling, machine learning, and information theory. He has contributed to ITU-R recommendations and reports in Study Group 3 (Propagation) including millimeter-wave propagation models. He is currently the Chairman of the ITU-R Correspondence Group 3K-6, which is responsible for studying the impact of higher frequencies (from 6 GHz to 450 GHz) on propagation models and related characteristics.